Introduction of Local Resonators to a Nonlinear Metamaterial with Topological Features

Joshua LeGrande[1'], Arun Malla[1'], Mohammad Bukhari[2], and Oumar Barry[1*]

[1]VibRo Lab, Department of Mechanical Engineering, Virginia Polytechnic University, Blacksburg, VA, 24060
[2]Department of Mechanical Engineering, Wayne State University, Detroit, MI, 48202
[*]Corresponding author, obarry@vt.edu
['] These authors contributed equally to this work.

January 24, 2024

Abstract

Recent work in nonlinear topological metamaterials has revealed many useful properties such as amplitude dependent localized vibration modes and nonreciprocal wave propagation. However, thus far, there have not been any studies to include the use of local resonators in these systems. This work seeks to fill that gap through investigating a nonlinear quasiperiodic metamaterial with periodic local resonator attachments. We model a 1-dimensional metamaterial lattice as a spring-mass chain with coupled local resonators. Quasiperiodic modulation in the nonlinear connecting springs is utilized to achieve topological features. For comparison, a similar system without local resonators is also modeled. Both analytical and numerical methods are used to study this system. The dispersion relation of the infinite chain of the proposed system is determined analytically through the perturbation method of multiple scales. This analytical solution is compared to the finite chain response, estimated using the method of harmonic balance and solved numerically. The resulting band structures and mode shapes are used to study the effects of quasiperiodic parameters and excitation amplitude on the system behavior both with and without the presence of local resonators. Specifically, the impact of local resonators on topological features such as edge modes is established, demonstrating the appearance of a trivial bandgap and multiple localized edge states for both main cells and local resonators. These results highlight the interplay between local resonance and nonlinearity in a topological metamaterial demonstrating for the first time the presence of an amplitude invariant bandgap alongside amplitude dependent topological bandgaps.

Keywords: Metamaterials, Nonlinear Vibrations, Perturbation Techniques

1 Introduction

Metamaterials are artificial engineered structures that are patterned with special configurations and material constituents [1–3]. These structures possess properties not found in naturally occurring materials, ranging from zero or negative values of standard engineering parameters (such as density and Poisson's ratio [1]), to nonlinear phenomena (such as gap solitons [4] and asymmetric wave propagation [5]). Metamaterials have a foundation in optics and electromagnetics, exploiting elastic and wave properties such as motion, deformations, stresses and mechanical energy [6, 7]. These concepts were later extended for elastic wave propagation [2] and acoustics [8]. The unusual features of metamaterials make them beneficial for numerous applications including vibration and noise control [9], energy harvesting [10], structural health monitoring [11], and acoustic diodes or rectifiers [12]. Within elastic media, metamaterials are usually patterned in periodic (phononic), quasiperiodic, or random structural configurations [13]. It was observed that periodic structures prevent waves from propagating through the structure at certain frequency ranges, known as bandgaps, through a phenomenon known as Bragg scattering. Therefore, low frequency waves can be banned from propagating through the structure, thus achieving significant vibration attenuation [2, 14]. However, since the Bragg scattering is restricted to certain lattice constants, only large structures can be controlled.

This large structure requirement can be counteracted by introducing local resonators into metamaterials [15]. Thus, applications of vibration attenuation can be extended to much smaller structures and applications. Local resonators are also capable of widening the original bandgap developed by Bragg scattering, as the

bandgap is directly influenced by the resonator parameters [16]. Furthermore, by introducing multiple resonators, additional multi-frequency bandgaps can be obtained [9, 17].

In addition, nonlinear elements can also be included in a metamaterial [18]. On top of the potential for improved bandgap performance, the introduction of nonlinearity also results in other interesting wave propagation phenomena such as gap solitons [4], dark and enveloped solitons [19], nonlinear cloaking [20–22], and wave nonreciprocity [23–25]. These phenomena can be applied for a host of applications. One option for the addition of nonlinearity to the metamaterial system is the use of nonlinear springs. These springs can have a combined linear and nonlinear stiffness or be essentially nonlinear, with nonlinear stiffness only. In the literature, study of nonlinear metamaterials is often focused on obtaining the band structure analytically or numerically [26, 27]. The former uses perturbation techniques (such as Lindstedt–Poincare [28], multiple scales [29] and homotopy analysis [30]), while the latter applies frequency and spectro-spatial analysis [31–34].

Quasiperiodic arrangements have also been shown to improve energy harvesting and vibration control through topologically protected modes. The investigation of topological phases of matter in metamaterials has shown the presence of robust topologically protected modes that do not propagate inside the bulk and are localized within lower dimensions [35]. One passive method for manifesting these topological modes is the breaking of spatial inversion symmetry while maintaining time-reversal symmetry [36–38]. This can be achieved by introducing quasiperiodic modulation into a structure using patterns such as the Aubry-André model as seen in [39–42]. This results in a spectrum that is analogous to the Hofstadter butterfly [43] with additional nontrivial topological bandgaps inside the bulk of propagating waves in periodic structures. These topological bandgaps host localized modes that can be beneficial in vibration mitigation [44] showing high displacement in a few cells while preventing wave propagation to other cells. Localization can also be moved along the metamaterial by topological pumping [45].

Further investigations have been made studying the effects of nonlinearity on topological metamaterials. The majority of these studies generally fall into one of two paths. The first path observes the effect of nonlinearity on a metamaterial that is topological in the linear regime. The second uses nonlinearity to strategically design metamaterials to induce topological properties in the metamaterial. In both cases, the amplitude dependence of the nonlinear response has led to studies in the frequency shift [46–48] and stability [49, 50] of topological edge states. One most common result of combining topological and nonlinear effects is the existence of solitons that are topologically robust [51–53].

Recent efforts in metamaterials have revealed interesting dynamical properties of locally resonant metamaterials with a wide variety of applications. Foremost among these is simultaneous vibration suppression and energy harvesting through the use of electromechanical resonators [34]. Modulating resonator parameters in quadratic [54] or quasiperiodic [42] patterns can even produce far superior energy harvesting performance over other metamaterials. In addition to enhanced harvesting energy, modulated resonators can be utilized to produce topological effects in metamaterials with simpler, non-topological host structures [39, 41]. Furthermore, local resonators have also proven useful in controlling waves through the design of two-dimensional waveguides [55] and electromechanical diodes [12]. Other applications in the nonlinear regime include control over breather propagation [56], and the strengthening of nonlinear phenomena such as frequency shifts and wave localization [57].

While the many valuable properties of local resonators have been widely studied, local resonators have not yet been introduced to nonlinear topological metamaterials. The aim of this work is to investigate the interactions between local resonance, nonlinear, and topological phenomena. In particular, we investigate a system that consists of a spring-mass chain with coupled local resonators and quasiperiodicity in the nonlinear connecting springs. The infinite chain model is solved analytically using the method of multiple scales, providing a closed form solution for the slow flow equations and nonlinear frequency correction factor. The method of harmonic balance is used to numerically estimate the behavior of a finite chain, providing insight into the natural frequencies and mode shapes of both main cells and local resonators. Both of these methods are used to study the effects of quasiperiodic parameters and excitation amplitude on the system behavior, focusing on the potential for vibration localization and control. The system is compared to a previously studied system lacking resonators [58], and the effect of local resonators on topological edge states and the behavior of local resonators in the proposed nonlinear quasiperiodic system is examined.

2 Modeling and Solution Methods

This work considers a 1-dimensional nonlinear locally resonant metamaterial with stiffness modulation in the main springs as shown in Fig. 1. The metamaterial is represented by a spring mass chain of identical masses, m, joined by modulated springs with linear and cubic nonlinear components. Each mass is coupled to a local resonator with mass, m_r and stiffness, k_r. Modulation in the main springs follows the Aubry-André Model
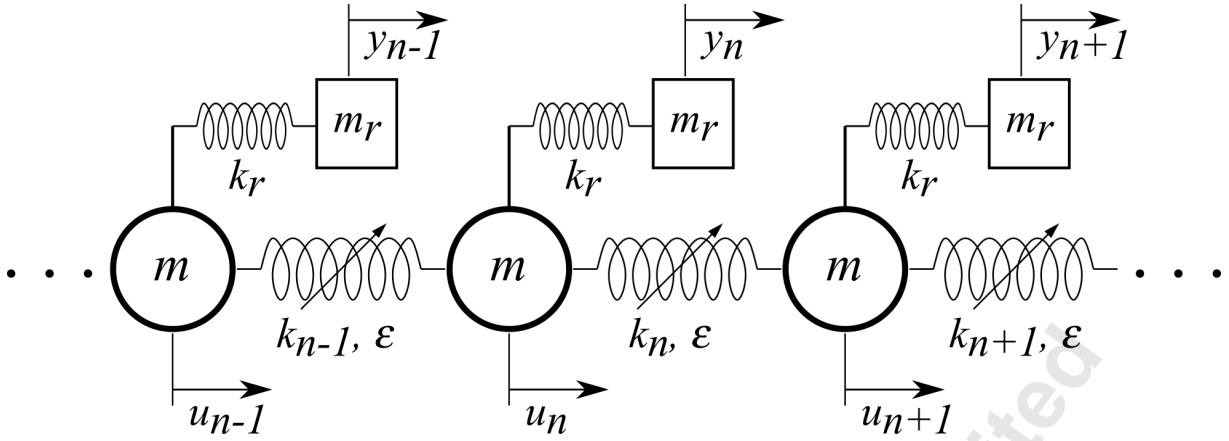
Figure 1: Schematic of nonlinear, quasiperiodic chain with local resonators.

such that the stiffness constant between mass n and mass $n + 1$ is defined as

$$k_n = k_0[1 + \lambda cos(2\pi n\theta + \phi)] \tag{1}$$

with average stiffness, k_0, and modulation amplitude, λ. This pattern is defined by its quasiperiodic parameter, θ, and phase shift, ϕ. It should be noted that $|\lambda| < 1$ in order to avoid negative values of stiffness k_n. Rational and irrational values of θ produce periodic and quasiperiodic patterns, respectively. The governing equations of motion for the nth mass and resonator are

$$m\ddot{u}_n + k_{n-1}(u_n - u_{n-1}) + k_n(u_n - u_{n+1}) + k_r(u_n - y_n) + \epsilon k_{n-1}(u_n - u_{n-1})^3 + \epsilon k_n(u_n - u_{n+1})^3 = 0 \tag{2}$$

$$m_r\ddot{y}_n + k_r(y_n - u_n) = 0 \tag{3}$$

where u_n and y_n are the displacements of the nth mass and resonator, respectively, and ϵ is a small dimensionless parameter defining the strength of the nonlinearity. These equations can be expressed compactly in matrix form for the jth unit cell as

$$\mathbf{M}\ddot{\mathbf{u}}_j + \mathbf{K}_{(0)}\mathbf{u}_j + \mathbf{K}_{(-1)}\mathbf{u}_{j-1} + \mathbf{K}_{(1)}\mathbf{u}_{j+1} + \epsilon\mathbf{f}^{NL} = 0 \tag{4}$$

where for a system with q masses in its unit cell, $\mathbf{M}$, $\mathbf{K}_{(0)}$, $\mathbf{K}_{(-1)}$, and $\mathbf{K}_{(1)}$ are $2q \times 2q$ mass and stiffness matrices, $\mathbf{u}_j$ is the $2q \times 1$ vector of mass and resonator displacements, and $\mathbf{f}^{NL}$ is the $2q \times 1$ nonlinear forcing vector.

2.1 The method of multiple scales

To derive the dispersion relation for an infinite chain, the perturbation method of multiple scales (MMS) is utilized with the fast time scale, $T_0 = t$, and the slow time scale, $T_1 = \epsilon t$. This method provides the simplest algebraic method for determining an analytical amplitude-wavenumber relationship. While using a first order approximation is accurate for weak nonlinearity, its accuracy will decrease with strong nonlinearity. At high amplitudes, a first order approximation is insufficient to detect higher order harmonics present in the response or to determine the stability of solutions. However, higher order harmonics and stability analysis are outside of the scope of this work and will be left for future work.

Using the MMS, we can assume expansions for the displacements in the form of

$$\mathbf{u}_j = \mathbf{u}_j^{(0)}(T_0, T_1) + \epsilon\mathbf{u}_j^{(1)}(T_0, T_1) + O(\epsilon^2) \tag{5}$$

and the time derivative can be expressed as

$$\frac{\partial^2}{\partial t^2} = D_0^2() + 2\epsilon D_0 D_1() + O(\epsilon^2) \tag{6}$$

where $D_n = \partial/\partial T_n$. Using these expansions, the equation of motion can be broken into linear and nonlinear components by order of ϵ yielding order ϵ^0

$$D_0^2\mathbf{M}\mathbf{u}_j^{(0)} + \mathbf{K}_{(0)}\mathbf{u}_j^{(0)} + \mathbf{K}_{(-1)}\mathbf{u}_{j-1}^{(0)} + \mathbf{K}_{(1)}\mathbf{u}_{j+1}^{(0)} = 0 \tag{7}$$

3

order ϵ^1

$$D_0^2 \mathbf{M}\mathbf{u}_j^{(1)} + \mathbf{K}_{(0)}\mathbf{u}_j^{(1)} + \mathbf{K}_{(-1)}\mathbf{u}_{j-1}^{(1)} + \mathbf{K}_{(1)}\mathbf{u}_{j+1}^{(1)} = -2D_0 D_1 \mathbf{M}\mathbf{u}_j^{(0)} - \mathbf{f}^{NL} \tag{8}$$

At order ϵ^0, the problem is linear, so the solution can be expressed as

$$\mathbf{u}_j^{(0)} = \frac{1}{2} A(T_1)\psi e^{i(\mu j - \omega_0 T_0)} + c.c. \tag{9}$$

where A is the amplitude, ψ is the mode shape, μ is the dimensionless wavenumber, ω_0 is the linear natural frequency, and $c.c.$ denotes the complex conjugate. Substituting the solution into the linear equation yields the linear eigenvalue problem

$$\omega_0^2 \mathbf{M}\psi = \mathbf{K}(\mu)\psi \tag{10}$$

where

$$\mathbf{K}(\mu) = \mathbf{K}_{(0)} + \mathbf{K}_{(-1)}e^{-i\mu} + \mathbf{K}_{(1)}e^{i\mu} \tag{11}$$

the solution of which obtains the linear dispersion relation and eigenvectors of the system.

Looking now to the nonlinear problem (i.e., the order ϵ problem), Eq. 8 is decoupled through the use of modal coordinates, then non-secular terms are isolated to derive the slow flow equations. Next, we introduce the polar form of the displacement amplitude

$$A_n = \alpha_n(T_1)e^{-i\beta_n(T_1)} \tag{12}$$

For a trimer lattice with $\theta = 1/3$, the slow flow equations are then solved to yield

$$\alpha'_n = 0 \tag{13}$$

$$\beta'_n = \frac{3\alpha_n^2 c_n(\mu)}{8m\omega_{0,n}\eta_n} \tag{14}$$

where

$$
\begin{aligned}
c_n(\mu) = &-2k_3\bar{\psi}_1\psi_3(|\psi_1|^2 + |\psi_3|^2)e^{-i\mu} + k_3\bar{\psi}_1^2\psi_3^2 e^{-2i\mu} + k_3\bar{\psi}_3^2\psi_1^2 e^{2i\mu} \\
&-2k_3\bar{\psi}_3\psi_1(|\psi_1|^2 + |\psi_3|^2)e^{i\mu} + (k_1+k_3)|\psi_1|^4 + (k_1+k_2)|\psi_2|^4 \\
&+(4k_1|\psi_2|^2 + 4k_3|\psi_3|^2 - 2k_1(\bar{\psi}_1\psi_2 + \bar{\psi}_2\psi_1))|\psi_1|^2 + (k_2+k_3)|\psi_3|^4 \\
&+(4k_2|\psi_3|^2 - 2k_1\bar{\psi}_1\psi_2 - (2k_1\psi_1 + 2k_2\psi_3)\bar{\psi}_2 - 2k_2\psi_2\bar{\psi}_3)|\psi_2|^2 \\
&-2k_2(\bar{\psi}_2\psi_3 + \bar{\psi}_3\psi_2)|\psi_3|^2 + k_1\bar{\psi}_1^2\psi_2^2 + (k_1\psi_1^2 + k_2\psi_3^2)\bar{\psi}_2^2 + k_2\bar{\psi}_3^2\psi_2^2
\end{aligned}
\tag{15}
$$

and

$$\eta_n = |\psi_1|^2 + |\psi_2|^2 + |\psi_3|^2 + \sqrt{\frac{m}{m_r}}(|\psi_4|^2 + |\psi_5|^2 + |\psi_6|^2) \tag{16}$$

with ψ_n being the nth element of the eigenvector associated with wavenumber, μ, and $\bar{\psi}_n$ being its complex conjugate. It can be shown that c_n is a purely real quantity.

The solution further allows us to express the nonlinear frequency in terms of the frequency correction factor, β'_n as

$$\omega_n = \omega_{0,n} + \epsilon\beta'_n \tag{17}$$

It is worth noting here that the frequency correction factor for this system is nearly identical to that presented in [58] for a system without local resonators. The primary distinction here is in the presence of the mass ratio term, η_n indicating that the frequency shift is directly influenced by the ratio of main cell mass to resonator mass.

2.2 The method of harmonic balance

While the method of multiple scales provides the dispersion relations for an infinite chain, this solution does not capture the edge modes present in the system. For this, an analysis of a finite chain is required. Although the method of multiple scales provides a simple algebraic approach to analyzing a single unit cell, it quickly becomes unruly when analyzing an entire chain of significant length. Instead, the harmonic balance method is used here following the procedures outlined in [47, 58]. This method also allows us to estimate the mode shapes for varying excitation amplitude. To examine these modes, a finite chain of $N = 42$ cells with free boundary conditions at each end is studied.

4

Beginning with the equations of motions in Eqs. 2 and 3, periodic solution forms for the displacement of the main cell and resonator masses are assumed as

$$u_n = a_n \cos\left(\omega t\right) + b_n \sin\left(\omega t\right) \tag{18}$$

$$y_n = c_n \cos\left(\omega t\right) + d_n \sin\left(\omega t\right) \tag{19}$$

where a_n, b_n, c_n, d_n are unknown displacement coefficients, and $\omega = 2\pi/T$ is the unknown assumed angular frequency with period T, resulting in $4N + 1$ unknowns.

A corresponding set of $4N+1$ nonlinear equations are obtained by substituting Eqs. 18 and 19 into the governing equations of motion, then setting the coefficient terms of $\cos\left(\omega t\right)$ and $\sin\left(\omega t\right)$ to 0. The final equation is provided by setting the L_2 norm of the displacement coefficients, $\mathbf{x} = \{a_1, b_1, c_1, d_1, ..., a_N, b_N, c_N, d_N\}^T$, equal to the total chain amplitude A.

$$\|\mathbf{x}\|_2 = A \tag{20}$$

For comparison to the infinite chain in the MMS solution, chain amplitude A is also used to define the Bloch wave amplitude, α_n, by $\alpha_n = A/\sqrt{\theta N}$. This is to ensure that when the wave solution is extended to a finite lattice with N masses, the resulting L_2 norm is equal to A [58].

The described set of $4N + 1$ algebraic nonlinear equations are solved numerically using a trust-region algorithm through MATLAB's "fsolve" function. To investigate the amplitude dependant effects of nonlinearity, the amplitude is first set to a small value, $A = 10^{-3}$. The initial guess for this case is the solution to the linear problem. Following this, A is increased in small increments, with each increase using the previous solution as the initial guess. Thus, the displacements and frequencies of the finite chain are calculated for a range of A.

3 Results and Discussions

Using the previously described solution methods, we examine selected variations of the proposed metamaterial. In this study, we consider a trimer lattice ($\theta = 1/3$) with the following parameters: $m = 1$ kg, $k_0 = 1$ N/m, $\lambda = 0.6$, $m_r = 0.2$ kg, $k_r = 0.3$ N/m, and $\epsilon = 0.1$. Although the system is only quasiperiodic for irrational θ values and periodic for rational θ values, the dispersion relations depend continuously on θ and can be accurately represented through sampling over rational values of θ. Several cases are studied, specifically a chain with linear springs or nonlinear springs, and with resonators or without resonators. While the linear dispersion relation will be given for a full range of phase variable, ϕ, the nonlinear dispersion relation will be given only for $\phi = 0.35\pi$ as more attention is given to its amplitude dependence than its phase dependence. Thus, the nonlinear dispersion relation is determined for varying displacement amplitudes, A, with set ϕ.

3.1 Band structure

The dispersion relations are shown in Fig. 2 for linear systems with and without resonators. The bulk passbands for an infinite chain, modeled from the unit cell and solved via MMS, are shown in blue. The natural frequencies of a finite chain, modeled with 42 masses and solved by harmonic balance, are overlaid as black lines. Comparing Fig. 2(a) and (b), the presence of the resonators in the linear chain has expected effects on the band structure as seen in previous studies [41, 42]. The dispersion band is split in two by a topologically trivial bandgap centered on the resonant frequency of the resonators. Above and below this bandgap, both passbands are split into additional passbands by topologically nontrivial bandgaps, resulting in a total of six passbands compared to the three passbands of the non-resonator case. The location and number of these nontrivial bandgaps are determined by the quasiperiodic parameter. Both with and without resonators, the frequencies of the finite chain reveal the presence of edge states that span the bandgaps. The frequency of these edge states is dependent on ϕ for the linear chain. Observing the case with resonators in Fig. 2(b) confirms that these edge states are present for nontrivial bandgaps only as there is no edge state present in the topologically trivial bandgap.

To observe the amplitude dependence, the nonlinear dispersion is plotted with increasing amplitude for the chains without and with resonators in Fig. 3. As in the linear case, the presence of resonators introduces a trivial bandgap, with nontrivial bandgaps on either side. In the nonlinear regime, frequencies shift upward with increasing amplitude for a positive (hardening) nonlinearity with $\epsilon = 0.1$ shown in Fig. 3(b). This affects several bandgap boundaries; however, the upper limit of the trivial bandgap shows no dependence on the amplitude, remaining constant as the amplitude increases. Edge mode frequencies also increase with amplitude, some approaching the neighboring bulk passbands at higher amplitudes. As they approach, edge modes eventually run tangent to the passband. While the majority of the finite chain modes remain within the infinite chain bulk passbands, the highest modes in each passband enter the bandgaps as amplitude
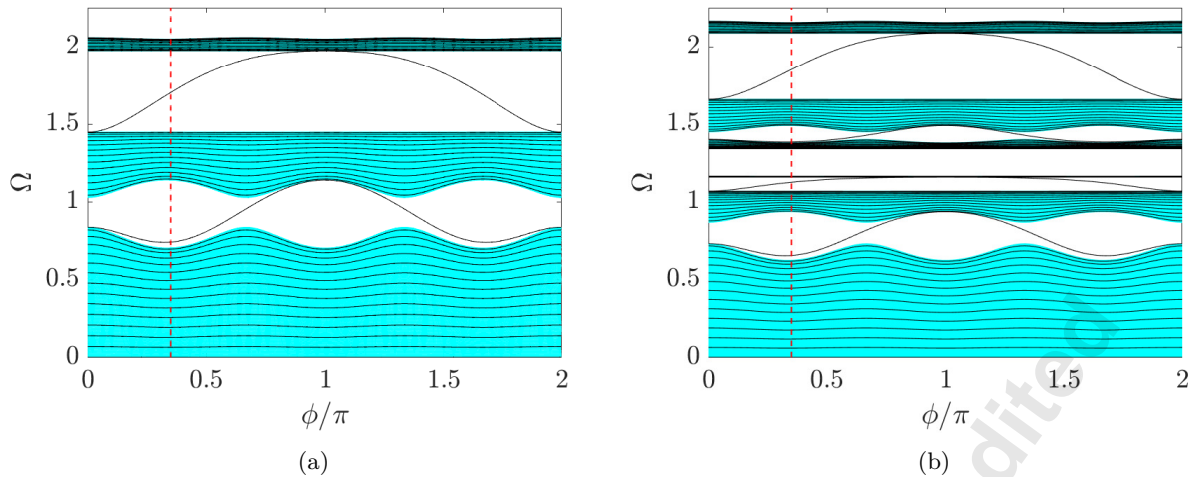
Figure 2: Effect of phase variable ϕ on the dispersion relations of a linear chain (a) without resonators and (b) with resonators.

increases and they are shifted to higher frequency. Previous works have shown that these modes, as well as the previously mentioned edge states, may display vibration localization [58]. Thus, the behavior of these modes is further investigated through the finite chain mode shapes acquired through harmonic balance.

When considering negative (softening) nonlinearity with $\epsilon = -0.1$, similar trends are identified except that frequencies are shifted downward instead of upward as depicted in Fig. 3(c). The bulk passbands shift downward in frequency, but the upper limit of the trivial bandgap remains unchanged. The edge modes shift downward causing some to enter or leave the bandgaps. For the fourth edge mode, we again see the edge mode shift in frequency until it approaches the adjacent passband. This time however, the edge mode approaches the lower passband rather than the upper passband with hardening nonlinearity. Since the frequency shift is downward, the edge modes starting at the lower frequency end of their bandgaps remain close to the lower passband and do not enter the bandgap. For example, the first edge mode is seen to move further into the bandgap with increasing amplitude in Fig. 3(b) under the influence of positive nonlinearity. However, for negative nonlinearity in Fig. 3(c), it remains close to the passband and never enters the bandgap as the amplitude increases. A significant difference to note is in the behavior of the modes that separate from the sixth passband. For positive nonlinearity, these are the highest frequency modes in the passband, and as the amplitude increases, they enter a bandgap and never return to the passband. But with negative nonlinearity, these are the lowest frequency modes in the passband, and because they shift downward, they enter the fifth bandgap and eventually join with the fifth passband. The effects of this behavior on the mode shapes will be detailed in the next section.

To further investigate the effect of the excitation amplitude on the band structure, we plot the natural frequencies in Fig. 4 over a range of quasiperiodic parameters at low amplitude ($A = 0$) in Fig. 4(a) and high ($A = 5$) amplitude with hardening and softening nonlinearity in Fig. 4(b)-(c), respectively. For each case, we observe that the bulk spectrum takes the expected form of the Hofstadter butterfly. At low amplitude, there is good agreement with previous studies [42]. The trivial bandgap is clearly displayed showing no dependence on the quasiperiodic parameter and no edge modes within it. Meanwhile, the topological bandgaps show great dependence on the quasiperiodic parameter. Looking to the higher amplitude cases, the previously noted effects of amplitude are confirmed. There is a slight but noticeable increase in frequency of the passbands for hardening nonlinearity and a decrease in frequency of the passbands for softening nonlinearity. These shifts are more significant for higher frequency modes. At the higher amplitude, the quasiperiodic parameter has a stronger impact on the location of the higher frequency bandgaps for hardening nonlinearity but a weaker impact for softening nonlinearity. For example, the uppermost "wing" of the butterfly with hardening nonlinearity in Fig. 4(b) has a maximum frequency of $\Omega = 3.94$ at $\theta = 0$ and drops down to $\Omega = 1.85$ at $\theta = 0.5$. When compared to the linear regime in Fig. 4(a), we see a range of $\Omega = 2.56 - 1.77$ over the same variation in quasiperiodic parameter. Furthermore, with softening nonlinearity in Fig. 4(c), the upper "wing" spans from $\Omega = 2.05 - 1.72$. The additional higher frequency modes entering the bandgaps can also be seen here. Fig. 4(b)-(c) shows that for high amplitude, the upper "wings" representing the bandgaps become less distinctive as more modes split from the bulk passbands and span the bandgaps. Additional curves also appear above the butterfly image in Fig. 4(b) indicating the modes that separated upward from the uppermost passband.
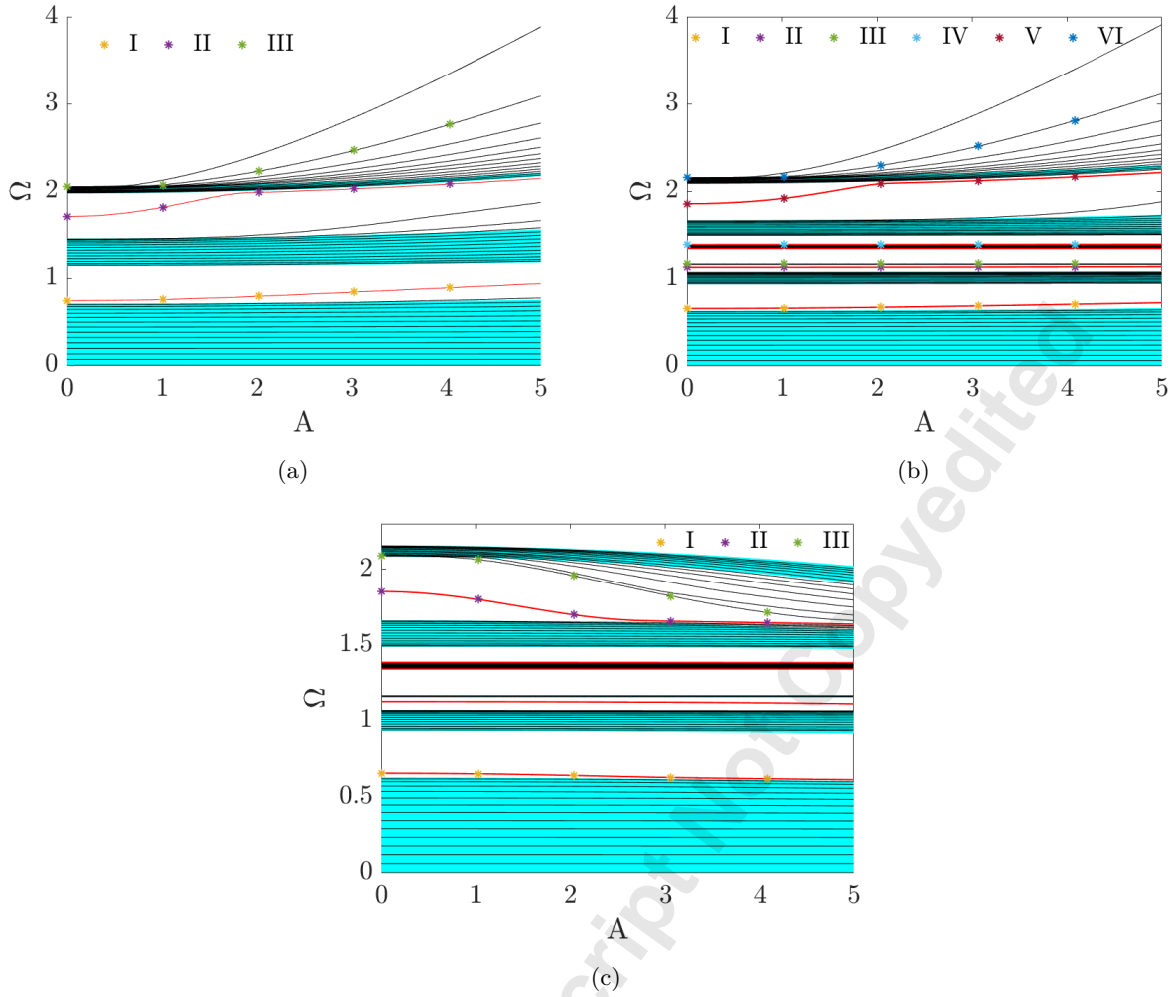
6

Figure 3: Effect of excitation amplitude A on the dispersion relations of a nonlinear chain at phase $\phi = 0.35\pi$ (a) without resonators, (b) with resonators and hardening nonlinearity, $\epsilon = 0.1$ and (c) with resonators and softening nonlinearity, $\epsilon = -0.1$.

3.2 Mode shapes

The effect of amplitude on the mode shapes of a nonlinear quasiperiodic chain without resonators is shown in Fig. 5. Mode shapes are normalized to the maximum displacement value for each amplitude, and the mode shapes for $A = 0.1$, 2.5, and 5 are outlined in black for clarity. Three selected mode branches are shown here: two edge states in Fig. 5(a) and (b) respectively, and the 41st mode in (c). The former two show that the edge modes result in localization to the ends of the chain. This localization is most pronounced at lower displacement amplitudes, where the effects of nonlinearity are negligible. However, as amplitude increases, the localization is affected to varying degrees. For the first edge mode in Fig. 5(a), increasing amplitude results in a more localized shape; while for the second edge mode in Fig. 5(b), higher amplitude results in a less localized shape. This can be explained through the band structure in Fig. 3(a) where the corresponding modes are highlighted with dotted curves and Roman numerals (I)-(III). Here, it is clear that while the first edge mode frequency increases with amplitude, it does not approach the second passband, remaining within the bandgap even at the highest value of A. On the other hand, the second edge mode does approach the third passband, running tangent to the passband at increased amplitude. Thus, its behavior is more similar to the bulk passband modes with less prominent localization. It can be concluded that localization is most significant when the mode frequency is within a bandgap and not approaching the edges. The phase ϕ will therefore have a significant impact on the effect of nonlinearity on mode shape localization, as it dictates the edge mode frequencies at low amplitude, and thus whether or not an edge mode will approach the next passband with increasing amplitude.

Meanwhile, the 41st edge mode, shown in Fig. 5(c), begins within the third passband, then increases with amplitude to enter the bandgap. Thus, its mode shape becomes more localized, similar to the first edge mode. This case also illustrates the localization of modes that begin at the upper edge of the passbands and
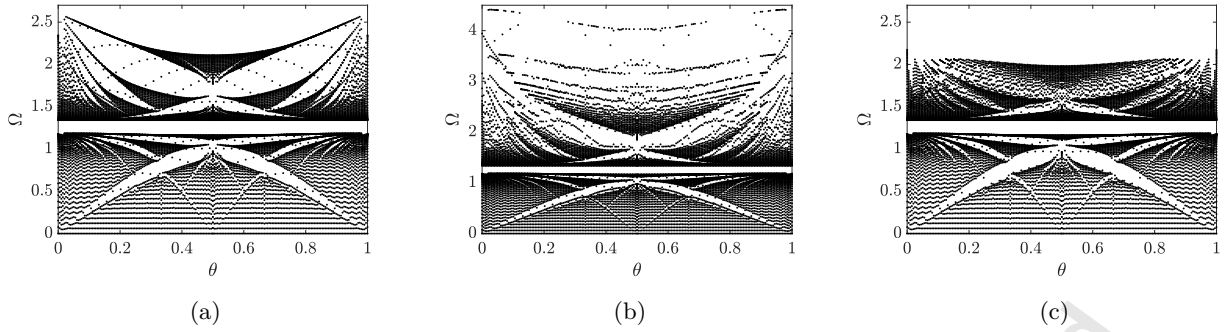
7

Figure 4: Natural frequency spectrum plotted over a range of quasiperiodic parameters, θ, with hardening nonlinearity, $\epsilon = 0.1$, at (a) low amplitude, $A = 0$ and (b) high amplitude, $A = 5$.
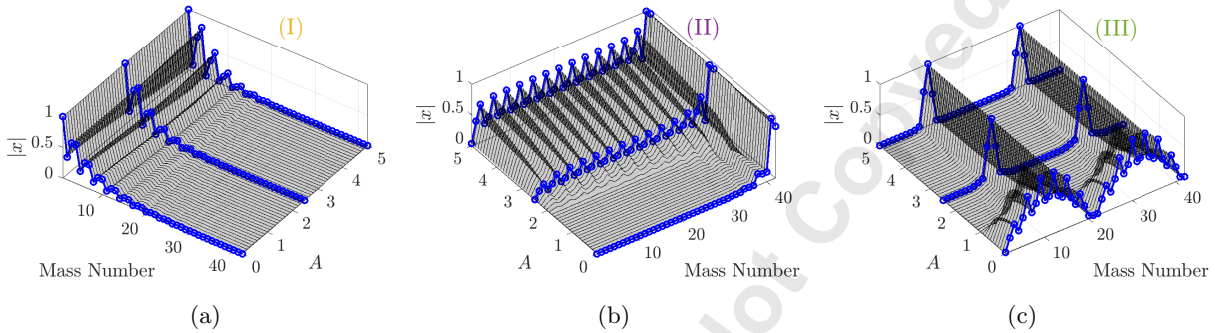

Figure 5: Effect of excitation amplitude A on selected mode shapes of a hardening nonlinear chain ($\epsilon = 0.1$) with $N = 42$ masses, without resonators, and $\phi = 0.35\pi$. (a) mode 15 (1st edge mode); (b) mode 29 (2nd edge mode); (c) mode 41.

enter the bandgaps at higher amplitude. The resulting mode shapes are localized to various points in the chain, forming discrete breathers. Breathers, which are solutions localized in space and periodic with time, have been established in prior work to emerge as modes at the edge of the passbands enter the nonlinear regime [58–60]. This is of particular interest in the second bandgap, where localized edge states and discrete breathers are both present. Overall, these observations for the chain without resonators are consistent with the previous work by Rosa et al. [58].

With the addition of resonators, many of the previous observations are still applicable. Though the band structure is split into six passbands rather than three, the behavior of the three passbands above and below the trivial bandgap is observed to follow similar patterns, with each set of passbands corresponding to the three passbands of the non-resonator case. However, there are some notable differences in the presence of resonators. To compare and contrast the effect of resonators and the behavior of passbands 1-3 and 4-6, the mode shapes of selected modes with varying displacement amplitude are shown in Fig. 6. Displacements of the main cells are marked with red circles, while the resonator displacements are marked with blue squares. All displacements are normalized to the maximum displacement of the main cells at each amplitude.

The response for passbands 1-3 with resonators is shown in Fig. 6(a)-(c). The first and second edge modes are shown in (a) and (b), respectively, while the 41st mode is shown in (c). In all modes, it is clear that the resonators have larger displacement amplitude relative to the main cells, and that the relative resonator amplitude increases slightly for higher amplitude. The resonator amplitude can also be observed to increase as the mode frequencies approach the trivial bandgap and thus the resonator natural frequency. The first edge mode is very similar to the case without resonator, with displacement localized to one end of the chain. The second edge mode, shown in Fig. 6(b), is similar to the non-resonator case at low amplitude, however, localization does not decrease as amplitude increases. The continued localization even at high amplitude may be explained by the band structure in Fig. 3(b) which also highlights the selected modes with dotted curves and Roman numerals (I)-(VI). Looking closely at the second edge mode, it can be seen that while the frequency does increase with amplitude, it remains away from the bandgap boundary and does not reach the point where it approaches and runs tangent to the third passband as in the non-resonator case. Thus, its behavior does not shift toward the passband behavior, and remains localized. The 41st mode in Fig. 6(c) also displays differences from the case with no resonator. While there are two clear peaks in the displacement, localization does not intensify as amplitude increases. This is due to the fact that, unlike the non-resonator
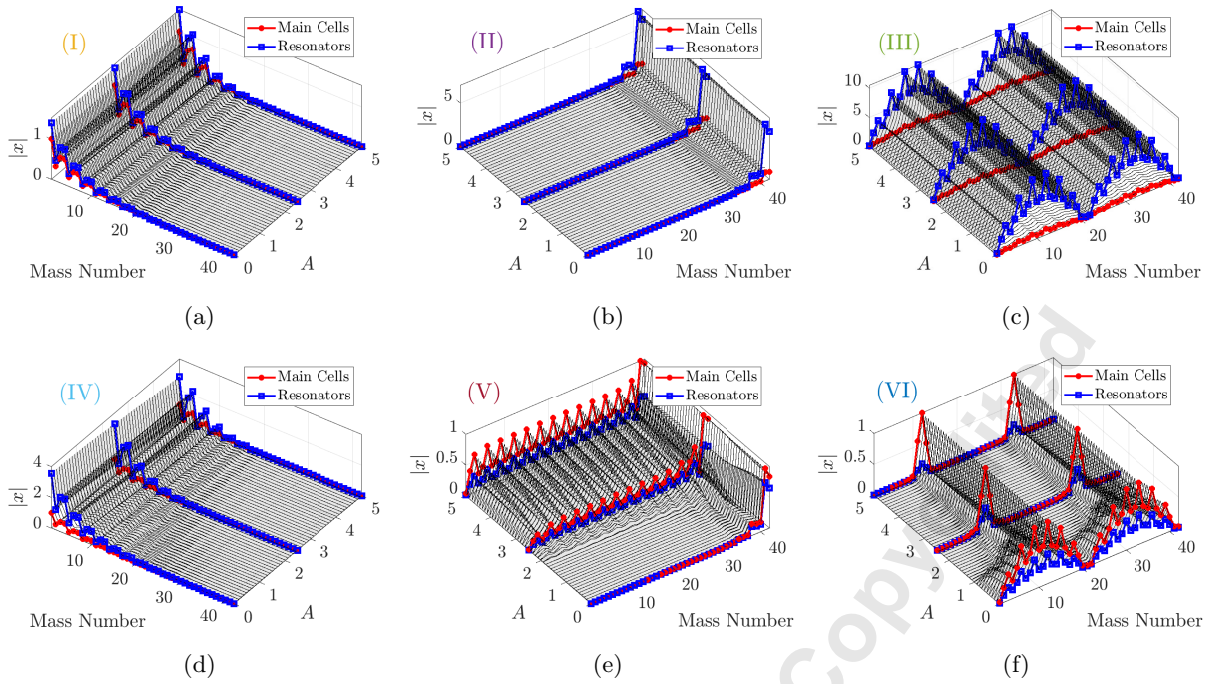
Figure 6: Effect of excitation amplitude A on selected mode shapes of a hardening nonlinear chain ($\epsilon = 0.1$) with $N = 42$ masses, with resonators, and $\phi = 0.35\pi$. (a) mode 15 (1st edge mode); (b) mode 29 (2nd edge mode); (c) mode 41; (d) mode 57 (3rd edge mode); (e) mode 71 (4th edge mode); (f) mode 83.

case, the 41st mode frequency does not separate from the bulk passband, and the mode shape is unaffected.

For passbands 4-6, the third and fourth edge modes are shown in Fig. 6(d) and (e), while the 83rd mode is shown in (f). Here, the displacement response is extremely similar to the case without resonator, including the formation of breathers in mode 83. Unlike passbands 1-3, the displacement of resonators relative to the main cells varies. For the third edge mode, resonator displacement is greater than main cell displacement, while for the other two modes, it is significantly less. This indicates that the resonator displacement decreases as we look at modes further from the trivial bandgap, matching the behavior in the lower three passbands.

One major difference between passbands 1-3 and 4-6 is that the edge modes for the lower three passbands have the resonators moving in phase with the main cells, while the resonators are out of phase for the upper three passbands. This is illustrated by Fig. 7, which shows mode shapes for the first and third edge modes with low displacement amplitude. Further exploration of the chain with resonators confirms that all modes below the trivial bandgap, and thus below the resonator natural frequency, have resonators in phase with the main cells, while above the trivial bandgap, resonators are out of phase. This matches observations of a similar system studied by LeGrande et al. [61].

For comparison, the response of some of these modes are also plotted for negative nonlinearity in Fig. 8. Shown here are the first and fourth edge modes in Fig. 8(a) and (b), respectively, and mode 72 in (c). These modes correspond to those in Fig. 3(c) that are highlighted with dotted curves and Roman numerals (I)-(III). Like with positive nonlinearity, the edge modes here show strong localization at low amplitudes. However, their response at high amplitudes varies. For the first edge mode, the influence of negative nonlinearity pushes the frequency into the bulk passband rather than into the bandgap. This leads to a decrease in localization at high amplitudes shown in Fig. 8(a). Looking to the fourth edge mode, it also significantly decreases in localization just as it did with positive nonlinearity. However, the edge mode reaches the lower passband at an amplitude near $A = 2.5$ whereas for the case of positive nonlinearity, the edge mode reaches the upper passband at a lower amplitude near $A = 2$. This causes the edge mode to remain localized at a higher amplitude for negative nonlinearity. This can be seen when comparing the response at amplitude $A = 2.5$ for positive nonlinearity in Fig. 6(e) and negative nonlinearity in Fig. 8(b). At this amplitude, there is a higher degree of localization for negative nonlinearity than for positive nonlinearity.

Another significant difference can be found in the response of the higher frequency modes that start in the bulk passband but show significant frequency shift. Figure 8(c) displays the mode shape associated with the 72nd mode which is the lowest frequency mode in the sixth passband. As previously mentioned, this mode undergoes a significant decrease in frequency separating from the bulk passband and entering into the bandgap. As it does, a centrally localized breather solution emerges in the mode shape. However, unlike with the case of positive nonlinearity, as the amplitude increases, the mode frequency eventually approaches the
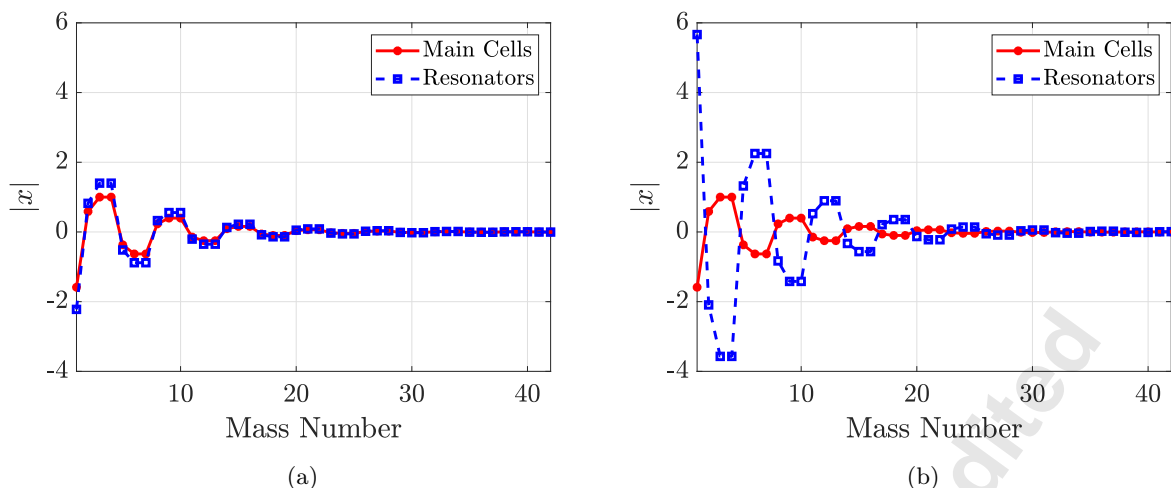
Figure 7: Selected mode shapes of nonlinear chain ($N = 42$) with resonators, $\phi = 0.35\pi$, $A = 0.1$. (a) Mode 15 (1st edge mode); (b) Mode 57 (3rd edge mode).
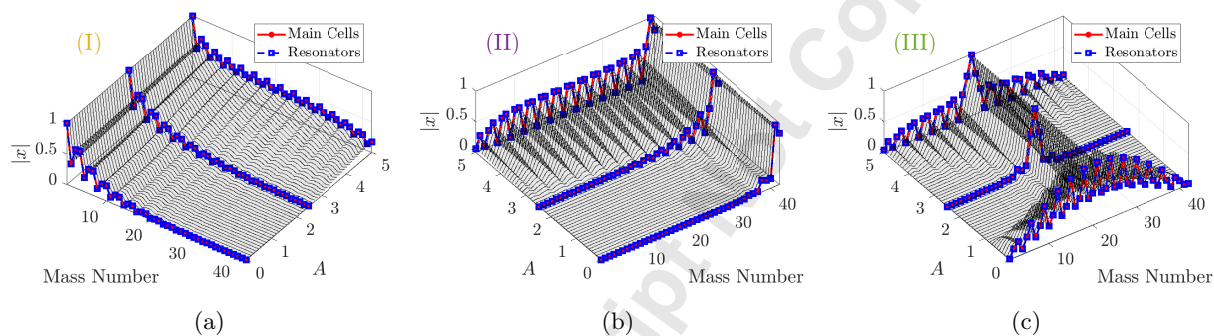

Figure 8: Effect of excitation amplitude A on selected mode shapes of a softening nonlinear chain ($\epsilon = -0.1$) with $N = 42$ masses, with resonators, and $\phi = 0.35\pi$. (a) mode 15 (1st edge mode); (b) mode 71 (4th edge mode); (c) mode 72.

fifth passband. As it does so, the degree of localization decreases and the wave begins to be dispersive again. This can be seen in Fig. 8(c) where the wave is more localized at amplitude $A = 2.5$ than it is at amplitude $A = 5$. This effectively produces an amplitude window within which breather solutions exist. At mid-level amplitudes, breathers will propagate with strong localization, but at lower or higher amplitudes, the wave will be dispersed along the chain. This demonstrates nonlinear mode pumping similar to topological pumping and driven mainly by the softening nonlinearity instead of patterning. This differs from the response with positive nonlinearity which produces breather solutions at all amplitudes above a set value.

4 Conclusion

This work investigated the effect of local resonators in a nonlinear metamaterial with quasiperiodic stiffness modulation. The proposed system was modeled as a 1-dimensional lattice of masses connected by cubic nonlinear springs. Linear and nonlinear stiffness of the connecting springs was modulated following the Aubry-André Model. Each main mass was coupled to a local resonator also modeled as a spring-mass system. Multiple techniques were applied to study this nonlinear system, with the response of an infinite chain model solved analytically through the method of multiple scales and the response of a finite chain estimated through the method of harmonic balance. The resulting frequency band structure and displacement mode shapes were compared to a similar system lacking local resonators to determine their effects.

In studying the proposed system, linear and nonlinear band structures were examined to determine the effects of phase variable and displacement amplitude. The results lacking resonators were found to be consistent with previous works, including the presence of nontrivial bandgaps, topological edge modes and amplitude dependence due to nonlinearity. With the addition of resonators, an additional trivial bandgap was observed, with nontrivial bandgaps appearing both below and above. Unlike the topological bandgaps,

this trivial bandgap appeared to be invariant with excitation amplitude. The resulting passbands below and above the trivial bandgap were shown to align closely with the passbands of the system without resonators. The presence of topological edge modes in nontrivial bandgaps was demonstrated, but as expected, no edge mode appeared within the trivial bandgap. It was also observed that some modes near the upper edge of the passbands shifted into the bandgaps as they entered the nonlinear regime.

The mode shapes of the system with and without resonators were also studied. Both with and without resonators, edge modes were shown to localize displacements to the ends of the chain. This localization was shown to change as edge modes entered the nonlinear regime. Modes that shifted deeper into the bandgaps showed increased localization, while edge modes that approached the edge of the passbands showed decreased localization. Meanwhile, some non-edge modes shifted into the bandgaps as they entered the nonlinear regime, resulting in discrete breathers. Examining mode shapes also confirmed that in the presence of resonators, the passbands above the trivial bandgap behaved almost identically to the passbands of the non-resonator system. While also similar, the behavior of modes below the trivial bandgap showed some differences to the non-resonator system. The displacement amplitude of resonators relative to the main cells was found to vary, with lower modes having resonator displacement greater than the main cells, while higher modes were the opposite. The phase of the local resonators was also found to be affected, with resonators being in phase with the main cells when below the trivial bandgap, and out of phase when above.

In conclusion, this work investigates the impact of local resonators on a nonlinear topological metamaterial and demonstrates that they can be seamlessly introduced to a nonlinear topological metamaterial. The proposed metamaterial was shown to combine the effects of nonlinearity, stiffness modulation and local resonators with little conflict. Traits such as amplitude dependence and localized topological edge modes continued to manifest, and new bandgaps were added by the resonators. The resulting increase in number of edge modes, passbands, and the presence of a trivial bandgap all serve to increase the versatility of the proposed metamaterial in both the linear and nonlinear regimes.

Acknowledgment

Data availability

The data sets generated and/or analyzed during the current study are available from the corresponding author on reasonable request.

Conflict of interest

The authors declare that they have no conflict of interest.

Appendix A   Method of multiple scales

To derive the dispersion relation for an infinite chain, the perturbation method of multiple scales (MMS) is utilized with the fast time scale, $T_0 = t$, and the slow time scale, $T_1 = \epsilon t$. We can assume expansions for the displacements in the form of

$$\mathbf{u}_j = \mathbf{u}_j^{(0)}(T_0, T_1) + \epsilon \mathbf{u}_j^{(1)}(T_0, T_1) + O(\epsilon^2) \tag{A.1}$$

and the time derivative can be expressed as

$$\frac{\partial^2}{\partial t^2} = D_0^2() + 2\epsilon D_0 D_1() + O(\epsilon^2) \tag{A.2}$$

where $D_n = \partial/\partial T_n$.

Using these expansions, the equation of motion can be broken into linear and nonlinear components by order of ϵ yielding order ϵ^0

$$D_0^2 \mathbf{M} \mathbf{u}_j^{(0)} + \mathbf{K}_{(0)} \mathbf{u}_j^{(0)} + \mathbf{K}_{(-1)} \mathbf{u}_{j-1}^{(0)} + \mathbf{K}_{(1)} \mathbf{u}_{j+1}^{(0)} = 0 \tag{A.3}$$

order ϵ^1

$$D_0^2 \mathbf{M} \mathbf{u}_j^{(1)} + \mathbf{K}_{(0)} \mathbf{u}_j^{(1)} + \mathbf{K}_{(-1)} \mathbf{u}_{j-1}^{(1)} + \mathbf{K}_{(1)} \mathbf{u}_{j+1}^{(1)} = -2 D_0 D_1 \mathbf{M} \mathbf{u}_j^{(0)} - \mathbf{f}^{NL} \tag{A.4}$$

11

At order ϵ^0, the problem is linear, so the solution can be expressed as

$$\mathbf{u}_j^{(0)} = \frac{1}{2} A(T_1) \psi e^{i(\mu j - \omega_0 T_0)} + c.c. \tag{A.5}$$

where A is the amplitude, ψ is the mode shape, μ is the dimensionless wavenumber, ω_0 is the linear natural frequency, and $c.c.$ denotes the complex conjugate. Substituting the solution into the linear equation yields the linear eigenvalue problem

$$\omega_0^2 \mathbf{M} \psi = \mathbf{K}(\mu) \psi \tag{A.6}$$

where

$$\mathbf{K}(\mu) = \mathbf{K}_{(0)} + \mathbf{K}_{(-1)} e^{-i\mu} + \mathbf{K}_{(1)} e^{i\mu} \tag{A.7}$$

the solution of which obtains the linear dispersion relation and eigenvectors of the system.

Looking now to the nonlinear equation, it is helpful to use modal analysis to decouple our system. We introduce new modal coordinates

$$\mathbf{z}_j = \Phi^H \mathbf{M}^{1/2} \mathbf{u}_j \tag{A.8}$$

$$\mathbf{z}_j^{(0)} = \frac{1}{2} [\Phi^H \mathbf{M}^{1/2} \psi] A e^{i(\mu j - \omega_0 T_0)} \tag{A.9}$$

where Φ^H is the Hermitian transpose of the matrix of eigenvectors. After making this transformation, we are left with the decoupled equations of motion

$$D_0^2 z_{j,n}^{(1)} + \omega_{0,n}^2 z_{j,n}^{(1)} = -D_0 D_1 [\Phi^H \mathbf{M}^{1/2} \psi]_n A_n e^{i(\mu j - \omega_{0,n} T_0)} - [\Phi^H \mathbf{M}^{-1/2} \mathbf{f}^{NL}]_n \tag{A.10}$$

where $[\ ]_n$ denotes the nth element in a vector.

To help identify non-secular terms, the nonlinear forcing term can be decomposed as

$$\mathbf{f}^{NL} = (\mathbf{F}_1^{NL} e^{-i\omega_{0,n} T_0} + \mathbf{F}_2^{NL} e^{-3i\omega_{0,n} T_0} + c.c.) e^{i\mu j} \tag{A.11}$$

Introducing this along with the polar form of the displacement amplitude

$$A_n = \alpha_n(T_1) e^{-i\beta_n(T_1)} \tag{A.12}$$

allows us to remove the secular terms from the RHS of Eq. A.10. Separating into real and imaginary components yields the slow flow equations:

$$[\Phi^H \mathbf{M}^{1/2} \psi]_n \omega_{0,n} \beta_n' \alpha_n e^{-i\beta_n} - [\Phi^H \mathbf{M}^{-1/2} \mathbf{F}_1^{NL}]_n = 0 \tag{A.13}$$

$$[\Phi^H \mathbf{M}^{1/2} \psi]_n \omega_{0,n} \alpha_n' e^{-i\beta_n} = 0 \tag{A.14}$$

where $'$ denotes a derivative with respect to T_1. Evaluation of the matrix components gives

$$[\Phi^H \mathbf{M}^{1/2} \psi]_n = m^{1/2} \eta_n \tag{A.15}$$

$$[\Phi^H \mathbf{M}^{-1/2} \mathbf{F}_1^{NL}]_n = \frac{3}{8} \alpha_n^3 e^{-i\beta_n} m^{-1/2} c_n(\mu) \tag{A.16}$$

where for a trimer lattice with $\theta = 1/3$,

$$\eta_n = |\psi_1|^2 + |\psi_1|^2 + |\psi_1|^2 + \sqrt{\frac{m}{m_r}} (|\psi_1|^2 + |\psi_1|^2 + |\psi_1|^2) \tag{A.17}$$

and

$$\begin{aligned}
c_n(\mu) = &-2k_3 \bar{\psi}_1 \psi_3 (|\psi_1|^2 + |\psi_3|^2) e^{-i\mu} + k_3 \bar{\psi}_1^2 \psi_3^2 e^{-2i\mu} \\
&+ k_3 \bar{\psi}_3^2 \psi_1^2 e^{2i\mu} - 2k_3 \bar{\psi}_3 \psi_1 (|\psi_1|^2 + |\psi_3|^2) e^{i\mu} \\
&+ (k_1 + k_3) |\psi_1|^4 + (k_1 + k_2) |\psi_2|^4 + (4k_1 |\psi_2|^2 \\
&+ 4k_3 |\psi_3|^2 - 2k_1 (\bar{\psi}_1 \psi_2 + \bar{\psi}_2 \psi_1)) |\psi_1|^2 + (k_2 + k_3) |\psi_3|^4 \\
&+ (4k_2 |\psi_3|^2 - 2k_1 \bar{\psi}_1 \psi_2 - (2k_1 \psi_1 + 2k_2 \psi_3) \bar{\psi}_2 \\
&- 2k_2 \psi_2 \bar{\psi}_3) |\psi_2|^2 - 2k_2 (\bar{\psi}_2 \psi_3 + \bar{\psi}_3 \psi_2) |\psi_3|^2 \\
&+ k_1 \bar{\psi}_1^2 \psi_2^2 + (k_1 \psi_1^2 + k_2 \psi_3^2) \bar{\psi}_2^2 + k_2 \bar{\psi}_3^2 \psi_2^2
\end{aligned} \tag{A.18}$$

with ψ_n being the nth element of the eigenvector associated with wavenumber, μ, and $\bar{\psi}_n$ being its complex conjugate. It can be shown symbolically that c_n is a purely real quantity.

The slow flow equations are then solved to yield solutions

$$\alpha'_n = 0 \tag{A.19}$$

$$\beta'_n = \frac{3\alpha_n^2 c_n(\mu)}{8m\omega_{0,n}\eta_n} \tag{A.20}$$

The solution further allows us to express the nonlinear frequency in terms of the frequency correction factor, β'_n as

$$\omega_n = \omega_{0,n} + \epsilon\beta'_n \tag{A.21}$$

References

[1] Katia Bertoldi, Vincenzo Vitelli, Johan Christensen, and Martin van Hecke. Flexible mechanical meta-materials. *Nature Reviews Materials*, 2(11):17066, 2017.

[2] Mahmoud I Hussein, Michael J Leamy, and Massimo Ruzzene. Dynamics of phononic materials and structures: Historical origins, recent progress, and future outlook. *Applied Mechanics Reviews*, 66(4):040802, 2014.

[3] Guancong Ma and Ping Sheng. Acoustic metamaterials: From local resonances to broad horizons. *Science Advances*, 2(2):e1501595, 2016.

[4] Yuri S Kivshar and Nikos Flytzanis. Gap solitons in diatomic lattices. *Physical Review A*, 46(12):7972, 1992.

[5] Bin Liang, Bo Yuan, and Jian chun Cheng. Acoustic diode: Rectification of acoustic energy flux in one-dimensional systems. *Physical Review Letters*, 46:104301, 103.

[6] Wenshan Cai and Vladimir M Shalaev. *Optical Metamaterials*, volume 10. Springer, 2010.

[7] Johan Christensen, Muamer Kadic, Oliver Kraft, and Martin Wegener. Vibrant times for mechanical metamaterials. *MRS Communications*, 5(3):453–462, 2015.

[8] Rosa Martínez-Sala, J Sancho, Juan V Sánchez, Vicente Gómez, Jaime Llinares, and Francisco Meseguer. Sound attenuation by sculpture. *Nature*, 378(6554):241–241, 1995.

[9] R Zhu, XN Liu, GK Hu, CT Sun, and GL Huang. A chiral elastic metamaterial beam for broadband vibration suppression. *Journal of Sound and Vibration*, 333(10):2759–2773, 2014.

[10] Ying Li, Evan Baker, Timothy Reissman, Cheng Sun, and Wing Kam Liu. Design of mechanical metamaterials for simultaneous vibration isolation and energy harvesting. *Applied Physics Letters*, 111(25):251903, 2017.

[11] Zheng Lu, Zixin Wang, Ying Zhou, and Xilin Lu. Nonlinear dissipative devices in structural vibration control: A review. *Journal of Sound and Vibration*, 423:18–49, 2018.

[12] Mohammad Bukhari and Oumar Barry. Broadband electromechanical diode: acoustic non-reciprocity in weakly nonlinear metamaterials with electromechanical resonators. *Journal of Vibration and Acoustics*, 145(2):021003, 2023.

[13] Younes Achaoui, Vincent Laude, Sarah Benchabane, and Abdelkrim Khelif. Local resonances in phononic crystals and in random arrangements of pillars on a surface. *Journal of Applied Physics*, 114(10):104503, 2013.

[14] Michael M Sigalas and Eleftherios N Economou. Elastic and acoustic wave band structure. *Journal of Sound and Vibration*, 158:377–382, 1992.

[15] Zhengyou Liu, Xixiang Zhang, Yiwei Mao, YY Zhu, Zhiyu Yang, Che Ting Chan, and Ping Sheng. Locally resonant sonic materials. *Science*, 289(5485):1734–1736, 2000.

[16] Liao Liu and Mahmoud I Hussein. Wave motion in periodic flexural beams and characterization of the transition between bragg scattering and local resonance. *Journal of Applied Mechanics*, 79(1):011003, 2012.

[17] GL Huang and CT Sun. Band gaps in a multiresonator acoustic metamaterial. *Journal of Vibration and Acoustics*, 132(3):031003, 2010.

[18] James M Manimala and CT Sun. Numerical investigation of amplitude-dependent dynamic response in acoustic metamaterials with nonlinear oscillators. *The Journal of the Acoustical Society of America*, 139(6):3365–3372, 2016.

[19] Neel Nadkarni, Chiara Daraio, and Dennis M Kochmann. Dynamics of periodic mechanical structures containing bistable elastic elements: From elastic to solitary wave propagation. *Physical Review E*, 90(2):023204, 2014.

[20] Bogdan-Ioan Popa, Lucian Zigoneanu, and Steven A Cummer. Experimental acoustic ground cloak in air. *Physical Review Letters*, 106(25):253901, 2011.

[21] Mohamed Farhat, Sebastien Guenneau, and Stefan Enoch. Ultrabroadband elastic cloaking in thin plates. *Physical Review Letters*, 103(2):024301, 2009.

[22] Amir Darabi, Ahmad Zareei, M-Reza Alam, and Michael J Leamy. Experimental demonstration of an ultrabroadband nonlinear cloak for flexural waves. *Physical Review Letters*, 121(17):174301, 2018.

[23] Xue-Feng Li, Xu Ni, Liang Feng, Ming-Hui Lu, Cheng He, and Yan-Feng Chen. Tunable unidirectional sound propagation through a sonic-crystal-based acoustic diode. *Physical Review Letters*, 106(8):084301, 2011.

[24] Chu Ma, Robert G Parker, and Benjamin B Yellen. Optimization of an acoustic rectifier for unidirectional wave propagation in periodic mass–spring lattices. *Journal of Sound and Vibration*, 332(20):4876–4894, 2013.

[25] Keegan J Moore, Jonathan Bunyan, Sameh Tawfick, Oleg V Gendelman, Shuangbao Li, Michael Leamy, and Alexander F Vakakis. Nonreciprocity in the dynamics of coupled oscillators with nonlinearity, asymmetry, and scale hierarchy. *Physical Review E*, 97(1):012219, 2018.

[26] Ali H Nayfeh. *Introduction to Perturbation Techniques*. John Wiley & Sons, 2011.

[27] Ali H Nayfeh and Dean T Mook. *Nonlinear Oscillations*. John Wiley & Sons, 2008.

[28] Raj K Narisetti, Michael J Leamy, and Massimo Ruzzene. A perturbation approach for predicting wave propagation in one-dimensional nonlinear periodic structures. *Journal of Vibration and Acoustics*, 132(3):031001, 2010.

[29] Kevin Manktelow, Michael J Leamy, and Massimo Ruzzene. Multiple scales analysis of wave–wave interactions in a cubically nonlinear monoatomic chain. *Nonlinear Dynamics*, 63(1-2):193–203, 2011.

[30] Mohammad H Abedin-Nasab, Mary V Bastawrous, and Mahmoud I Hussein. Explicit dispersion relation for strongly nonlinear flexural waves using the homotopy analysis method. *Nonlinear Dynamics*, 99(1):737–752, 2020.

[31] R Ganesh and Stefano Gonella. Spectro-spatial wave features as detectors and classifiers of nonlinearity in periodic chains. *Wave Motion*, 50(4):821–835, 2013.

[32] WJ Zhou, XP Li, YS Wang, WQ Chen, and GL Huang. Spectro-spatial analysis of wave packet propagation in nonlinear acoustic metamaterials. *Journal of Sound and Vibration*, 413:250–269, 2018.

[33] Mohammad Bukhari and Oumar Barry. On the spectro-spatial wave features in nonlinear metamaterials with multiple local resonators. In *ASME 2018 International Design Engineering Technical Conferences and Computers and Information in Engineering Conference*. American Society of Mechanical Engineers, 2019.

[34] Mohammad Bukhari and Oumar Barry. Simultaneous energy harvesting and vibration control in a nonlinear metastructure: A spectro-spatial analysis. *Journal of Sound and Vibration*, 473:115215, 2020.

[35] Guancong Ma, Meng Xiao, and Che Ting Chan. Topological phases in acoustic and mechanical systems. *Nature Reviews Physics*, 1(4):281–294, 2019.

[36] S Hossein Mousavi, Alexander B Khanikaev, and Zheng Wang. Topologically protected elastic waves in phononic metamaterials. *Nature Communications*, 6(1):1–7, 2015.

[37] Marco Miniaci, RK Pal, B Morvan, and M Ruzzene. Experimental observation of topologically protected helical edge modes in patterned elastic plates. *Physical Review X*, 8(3):031074, 2018.

[38] Rajesh Chaunsali, Chun-Wei Chen, and Jinkyu Yang. Subwavelength and directional control of flexural waves in zone-folding induced topological plates. *Physical Review B*, 97(5):054307, 2018.

[39] Matheus IN Rosa, Yuning Guo, and Massimo Ruzzene. Exploring topology of 1d quasiperiodic metastructures through modulated lego resonators. *Applied Physics Letters*, 118(13):131901, 2021.

[40] David J Apigo, Kai Qian, Camelia Prodan, and Emil Prodan. Topological edge modes by smart patterning. *Physical Review Materials*, 2(12):124203, 2018.

[41] Yiwei Xia, Alper Erturk, and Massimo Ruzzene. Topological edge states in quasiperiodic locally resonant metastructures. *Physical Review Applied*, 13(1):014023, 2020.

[42] Joshua LeGrande, Mohammad Bukhari, and Oumar Barry. Effect of electromechanical coupling on locally resonant quasiperiodic metamaterials. *AIP Advances*, 13(1):015112, 2023.

[43] Xiang Ni, Kai Chen, Matthew Weiner, David J Apigo, Camelia Prodan, Andrea Alù, Emil Prodan, and Alexander B Khanikaev. Observation of hofstadter butterfly and topological edge states in reconfigurable quasi-periodic acoustic crystals. *Communications Physics*, 2(1):1–7, 2019.

[44] Raj Kumar Pal, Matheus IN Rosa, and Massimo Ruzzene. Topological bands and localized vibration modes in quasiperiodic beams. *New Journal of Physics*, 21(9):093017, 2019.

[45] Matheus IN Rosa, Raj Kumar Pal, José RF Arruda, and Massimo Ruzzene. Edge states and topological pumping in spatially modulated elastic lattices. *Physical Review Letters*, 123(3):034301, 2019.

[46] Raj Kumar Pal, Javier Vila, Michael Leamy, and Massimo Ruzzene. Amplitude-dependent topological edge states in nonlinear phononic lattices. *Physical Review E*, 97(3):032209, 2018.

[47] Javier Vila, Glaucio H Paulino, and Massimo Ruzzene. Role of nonlinearities in topological protection: Testing magnetically coupled fidget spinners. *Physical Review B*, 99(12):125116, 2019.

[48] Amir Darabi and Michael J Leamy. Tunable nonlinear topological insulator for acoustic waves. *Physical Review Applied*, 12(4):044030, 2019.

[49] Joshua R Tempelman, Kathryn H Matlack, and Alexander F Vakakis. Topological protection in a strongly nonlinear interface lattice. *Physical Review B*, 104(17):174306, 2021.

[50] Rajesh Chaunsali, Haitao Xu, Jinkyu Yang, Panayotis G Kevrekidis, and Georgios Theocharis. Stability of topological edge states under strong nonlinear effects. *Physical Review B*, 103(2):024106, 2021.

[51] David DJM Snee and Yi-Ping Ma. Edge solitons in a nonlinear mechanical topological insulator. *Extreme Mechanics Letters*, 30:100487, 2019.

[52] Rajesh Chaunsali and Georgios Theocharis. Self-induced topological transition in phononic crystals by nonlinearity management. *Physical Review B*, 100(1):014302, 2019.

[53] Bryan Gin-ge Chen, Nitin Upadhyaya, and Vincenzo Vitelli. Nonlinear conduction via solitons in a topological mechanical insulator. *Proceedings of the National Academy of Sciences*, 111(36):13004–13009, 2014.

[54] M Alshaqaq and A Erturk. Graded multifunctional piezoelectric metastructures for wideband vibration attenuation and energy harvesting. *Smart Materials and Structures*, 30(1):015029, 2020.

[55] Filippo Casadei, Tommaso Delpero, Andrea Bergamini, Paolo Ermanni, and Massimo Ruzzene. Piezoelectric resonator arrays for tunable acoustic waveguides and metamaterials. *Journal of Applied Physics*, 112(6):064902, 2012.

[56] Mohammad A Bukhari, Oumar R Barry, and Alexander F Vakakis. Breather propagation and arrest in a strongly nonlinear locally resonant lattice. *Mechanical Systems and Signal Processing*, 183:109623, 2023.

[57] Mohammad Bukhari and Oumar Barry. Substantial frequency conversion at long-wavelength limit in metamaterial with weakly nonlinear local electromechanical resonators: Analytical, computational, and experimental study. *International Journal of Non-Linear Mechanics*, 147:104226, 2022.

[58] Matheus IN Rosa, Michael J Leamy, and Massimo Ruzzene. Amplitude-dependent edge states and discrete breathers in nonlinear modulated phononic lattices. *New Journal of Physics*, 25(10):103053, 2023.

[59] Sergej Flach and Charles R. Willis. Discrete breathers. *Physics reports*, 295(5):181–264, 1998.

[60] Neil Boechler, Georgios Theocharis, and C Daraio. Bifurcation-based acoustic switching and rectification. *Nature Materials*, 10(9):665, 2011.

[61] Joshua LeGrande, Mohammad Bukhari, and Oumar Barry. Topological properties and localized vibration modes in quasiperiodic metamaterials with electromechanical local resonators. In *International Design Engineering Technical Conferences and Computers and Information in Engineering Conference*, volume 86311, page V010T10A004. American Society of Mechanical Engineers, 2022.